Fabrication, Structural and Photocatalytic Studies of Titanium Dioxide urchin-like Nanoparticles for the Removal of Organic Dye from Aqueous Media

Hanan.M.Yousef, M.Y.Nassar, Ismaeel.M.Ali and H.M.Aly
Chemistry Department, Faculty of Science, Benha University, Benha, Egypt
E-mail: hisham.ali@fsc.bu.edu.eg

Abstract

One-pot hydrothermal treatment using ethylene glycol (EG) at 180 °C for 12 h has been confirmed to effectively generate titanium dioxide urchin-like nanoparticles. X-Ray diffractometry (XRD), Field emission scanning electron microscopy (FE-SEM), and Fourier transform infrared spectroscopy (FT-IR) were applied to characterize the structure and morphology of the as-prepared titanium dioxide after calcination at different temperatures for 2 h. According to XRD analysis, the synthesized calcined titanium dioxide has average crystallite sizes between 13.4 and 17.7 nm. The photocatalytic behavior of the prepared titanium dioxide nanoparticles was examined utilizing methylene blue dye. The process of photodegradation is performed under different experimental parameters such as the influence of contact time, initial dye concentration, photocatalyst dose and temperature. The MB photodegradation kinetics was found to follow the pseudo-first-order model with $R^2 > 0.99$. Thermodynamic parameters for the photodegradation system showed that the photodegradation process is spontaneous, endothermic and favorable at high temperatures.

Keywords: Hydrothermal method, Titanium dioxide Nanoparticles, Photodegradation process, kinetics, Methylene blue dye (MB).

1. Introduction

The acceleration of industrialization has led to a significant increase in the severity of water pollution, resulting in adverse impacts on the environment. As per recent reports, a significant proportion of industries release approximately 70% of their waste materials into water bodies without undergoing any form of treatment or refinement [1]. The critical issue of solving water pollution through cost-effective, energy-efficient, and high-performance methods requires immediate attention. The elimination of organic pollutants is of considerable importance in the realm of water conservation. Solar energy is widely regarded as a highly desirable source of green and clean energy for human use due to its inexhaustible nature, safety, and reliability [2]. So far, traditional techniques have been employed to deal with these issues, such as flocculation-condensation [3], oxidation or ozonation [4], membrane separation [5], adsorption [6], and reverse osmosis [7]. However, these techniques cannot completely remove or seriously eliminate organic pollutants in the water. Dye is a common industrial organic contaminant. Methylene blue (MB), a cationic dye, is widely used in industry and medicine. MB effluent has various health risks and affects the ecosystem [8].

In recent years, an attractive method for water purification has been the efficient development of photocatalytic degradation of organic dyes in wastewater by catalysts. At the catalyst's surface, a heterogeneous reaction known as the photocatalytic reaction occurs. Through a variety of methods, including excitation, redox reactions, and recombination, it is to accelerate the reduction of light energy into chemical energy. This reaction also aims to create a potential equilibrium between the

catalyst's Fermi level of energy and the surface adsorbents [9-12]. Photocatalytic degradation of dyes into non-toxic products such as CO_2 and H_2O is a green method owing to the non-use of polluting substances. Titanium dioxide (TiO_2) is utilized in photocatalysis, adsorption [13], dye-sensitized solar cells [14], batteries [15], gas sensing [16], and cancer treatment [17]. Titanium dioxide (TiO_2) is a significant semiconductor material of transition metal oxide with a direct band gap of approximately 3.2 eV. At UV light irradiation, TiO_2 undergoes excitation, in which electrons are promoted from the valence band to the conduction band, leading to the formation of electron-hole pairs. The activation of surrounding chemical species is facilitated by the formation of electron-hole pairs, which then induce chemical reactions [18,19]. However, TiO_2 exhibits certain constraints, primarily attributable to the rapid recombination of (e^-/h^+) pairs produced and a limited spectrum of absorbed wavelength [20]. Enhancing the performance of charge separation requires a systematic approach to the structural design of the photocatalyst. Compared to TiO_2 with unmodified morphology, TiO_2 with different dimensionalities, including nanospheres (0D) [21], nanotubes (1D) [22], and nanosheets (2D) [23], have demonstrated enhanced photocatalytic efficacy. There are various advantages to using three-dimensional (3D) TiO_2 structures over low-dimensional structures, such as sea urchin- and nanoflower-like morphologies. High specific surface area, low aggregation, and simple separation of particles from solutions are a few of these benefits [24,25]. Typically, a greater specific surface area facilitates the creation and transmission of photocarriers, as well as the adherence of reactants to the surface, while concurrently enhancing the sol-gel, hydrothermal, and solvothermal processes have

all been used for the synthesis of TiO_2 materials [26,27].The hydrothermal method is a frequently used technique due to its ability to regulate the formation of nanostructures through the influence of reaction temperature and time, active fill level in the pressure vessel, or solvent used for the reaction. The use of structure-directing agents or templates is not necessary with this technique [28,29]. So, using a simple EG-assisted hydrothermal technique, 3D sea urchin-like TiO_2 structures were achieved in this research. Systematically examining the role of calcination temperature on the character of sea urchin-like shapes. Additionally, its experimental photocatalytic activity was evaluated for methylene blue (MB) aqueous solution degradation. Based on the effects of several elements such as contact time, dye concentration, and photocatalyst dose on photocatalytic degradation, process optimization is examined.

2. Experimental Methods
2.1 Materials

Tetrabutyl Orthtitanate (TBOT), hydroxide of sodium (NaOH), ethane-1,2-diol (EG), hydrochloric acid (HCl), and methylene blue (MB) were purchased from Sigma-Aldrich. The studies were done with deionized water. The chemicals used in the experiment were all analytical grades and used without further purification. The structure of Methylene Blue (MB) dye is shown in Fig.1.

Fig. 1 Structure of MB dye.
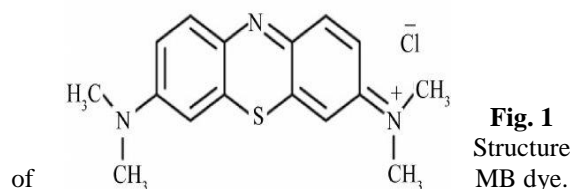
2.2 Fabrication of titanium dioxide (TiO_2) nanoparticles via the hydrothermal method

Ethylene glycol-assisted hydrothermal treatment with TBOT as a titanium source produced 3D sea urchin-like TiO_2 structures. 20 ml of 1 M NaOH aqueous solution and 0.35 ml of TBOT are typically combined and stirred. Ultrasonically sonicating the solution for 5 min released more TBOT. After that, 40 ml of EG was added to the mixture, and it was thoroughly stirred. The Teflon-lined hydrothermal reaction vessel heated the white solution for 12 h at 180 °C. The white precipitates that formed when the vessel cooled down were recovered by centrifugation and repeatedly washed with 0.1 M HCl and deionized water until the supernatant's pH was ~7. To facilitate the crystallization of TiO_2, the samples that were collected were dried out over 12 h at 50 °C and then calcined for 2 h in the air at various temperatures. The samples that were created have the following terms: T-350 and T-550 which indicate sea urchin-like TiO_2 calcined at 350 and 550 °C, respectively.

2.3 Photodegradation studies

The nanoparticles were tested for UV light-induced photocatalytic decomposition of MB solution. Photocatalysts were dissolved in a water solution of MB (20 mg/L) at an amount of 5 mg per 50 mL. The mixture was magnetically stirred (at a speed of around 400 rpm) in the dark for 45 min to get about the adsorption-desorption balance before UV light treatment. MB's photocatalytic decomposition started by exposing the reaction solution using a commercial 60W xenon lamp (λ max = 365 nm). Using a Jasco-670 UV-visible spectrophotometer calibrated at 664 nm, the amount absorbed by a catalyst-free treatment dye solution was determined, and it was examined with the maximum MB absorbance. Different photocatalytic conditions, including contact time, initiating concentrations, photocatalyst dosage, and temperatures, were examined to improve comprehension of the resulting nanoparticles' catalytic activity. The titanium dioxide photocatalyst's catalytic activity was carried out under the same conditions by adding 0.05 g of graphene to TiO_2 after calcination. For all samples, the efficiency of photocatalytic decomposition (DE) was calculated via the equation, % MB decomposition = $[(C_0 - C_t) \times 100\%]/C_0$, where C_0 is the beginning amount of the MB (mg L^{-1}) at zero time, and C_t is MB amount at a given time (mg L^{-1}). The durability of TiO_2 calcined at various temperatures was examined for MB decomposition across a five-cycle period. In the creation of the cycle decline, TiO_2 calcined at different temperatures was obtained and purified. The material was produced and dried at 60 °C for 12 h. Determining solution dye concentrations used the MB dye's distinguished absorption at 664 nm.

3. Results and discussion
3.1. X-ray studies

The XRD pattern was investigated using Cu- Kα irradiation source (λ = 1.5406Å) for powder X-ray diffraction (XRD) using 18 KW Bruker model D8 Advance diffractometer. Fig. 2 reveals the crystallinity and geometry of the calcined titanium dioxide (T-350 and T-550 samples). NPs at 2θ values of 25.06°, 37.54°,48.30°, 54.89°, and 62.59°, which correspond to the (101), (004), (200), (211), and (200) crystal planes, respectively, in agreement with JCPDS-00-001-0562. The average crystallite sizes of the calcined TiO_2 sample were calculated using the Debye-Scherer formula [30] (equation 1).

$$D = 0.9\lambda/\beta\cos\theta \qquad (1)$$

Where λ is the wavelength of X-ray, β is the full width at half-maximum and θ is the angle of diffraction. For T-350 and T-550, the average titanium dioxide crystallite size (D) is found to be 13.4 nm and 17.7 nm, respectively.

3.2. FT-IR studies

In fig. 3(a-b) displays the functional groups of the calcined titanium dioxide (T-350 and T-550 samples) using Fourier transform infrared (FI-IR). The spectrum shows several peaks at 3405.06, 2924.01, 3260.35, 1618.36, and 463.73 cm^{-1}. Hydroxyl group (Ti-OH) stretching vibrations are asymmetrical and symmetrical at 3405.06 and 3260.35 cm^{-1}. Weak bands at 2924.01 cm^{-1} could be due to the characteristic frequencies of organic residues that were not all washed away by ethanol and purified water. These frequencies could be identified as C-H vibrations that stretch alkane groups. At 1618.36 and 463.73 cm^{-1}, respectively, the Ti-O bending mode and the deformative vibration of the Ti-OH stretching mode may be seen. At 1618.36 cm^{-1} shows that the sample contains moisture. The impacts from the anatase titania are visible in the peaks at 463.73 and 438.86 cm^{-1} for pure TiO$_2$.

3.3. Morphological studies

Fig. 4(a-b) exhibits the morphology of the calcined titanium dioxide (T-350 and T-550 samples) under a field emission scanning electron microscope (FE-SEM). Sea urchin-like structures were produced by 3D micro-sized TiO$_2$ that had spindle-like structures protruding from a central core. It is also possible to create two- and one-dimensional (2D) materials using hydrothermal processes [23,31,32]. T-350 shown in Figs. 4a exhibited sea urchin-like structures with pointed spindles. However, molten aggregates were obtained for T-550 as in Fig. 4b. Thus, the temperature of the calcination process can change the morphology of TiO$_2$, leading to significant deformation. The EDX results (Fig. 4c) confirmed the purity of the samples through the detection of Ti and O elements.

4. Photocatalytic performance

The effect of heat treatment of the catalyst was studied for samples treated at 350°C and 550°C. Fig. 5. shows that the photocatalytic decomposition followed the order; T-350 > T-550, and the MB removals reached up to 81.42 and 69.68%, respectively, after 270 min. Graphene (0.05 g) was utilized to inhibit the electron/hole pair recombination [20]. As demonstrated in Fig. 6, the degradation rate of MB dye over TiO$_2$ calcined at different temperatures was greatly enhanced by adding graphene; not only was the time of degradation decreased from 270 min to 90 min, but also the photocatalytic activity was greatly increased to 95.84 and 86.9%, respectively. This could be because graphene plays the role of an electron acceptor that accelerates the interfacial electron-transfer process from photocatalyst materials, which

strongly hinders the recombination of charge carriers and thus improves photocatalytic activity. The procedure of putting photoactive spots on its surface is made easier by the dispersion of the oxygenated functional groups on its surface [33]. Graphene Can provide very high mobility to the photogenerated electrons and reduce e$^-$/h$^+$ recombination [34].

4.1 The Influence of contact time

The effect of contact time of the as-prepared photocatalysts (T-350 and T-550) over the MB dye's decomposition under UV light was investigated at PH (7.0 ± 0.1),0.005 g photocatalyst dose and an initial MB dye concentration of 15 mg/L. Fig. 7 illustrates the time-dependent decomposition of MB when exposed to UV light when catalysts are present (T-350 and T-550) with uniform irradiation over time. The rate of uptake was rapid in the beginning and gradually became in the later stages until saturation state, as shown in Fig. 7. As seen after 270 min irradiation, MB solution decomposition over T-350 and T-550 reached 81.92 and 71.12%, respectively. The results show that when exposure time increased, MB's breakdown increased as well.
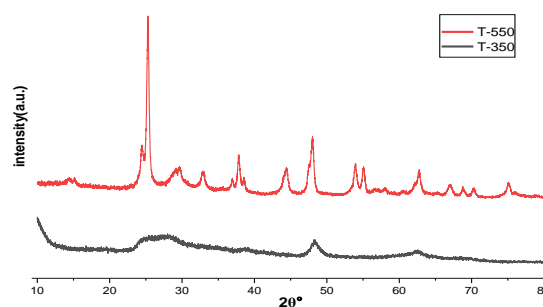

Fig. (2) XRD patterns of calcined TiO$_2$ (T-350 and T-550 samples)
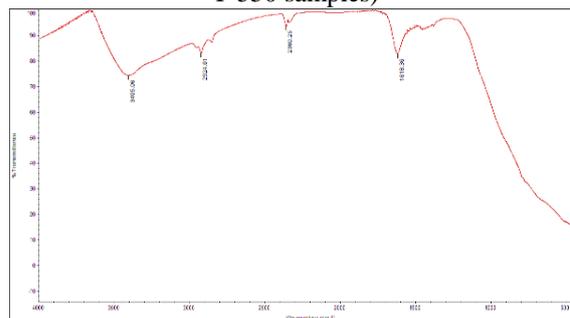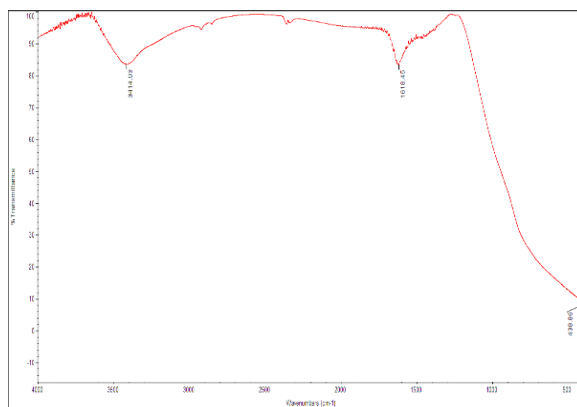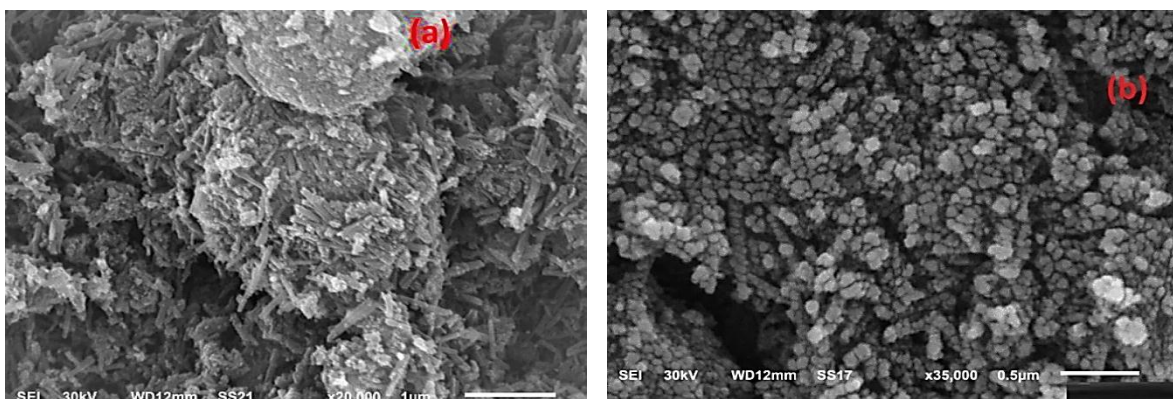

Fig. 3(a) FT-IR spectra of titanium dioxide calcined at 350 ºC (T-350 sample)
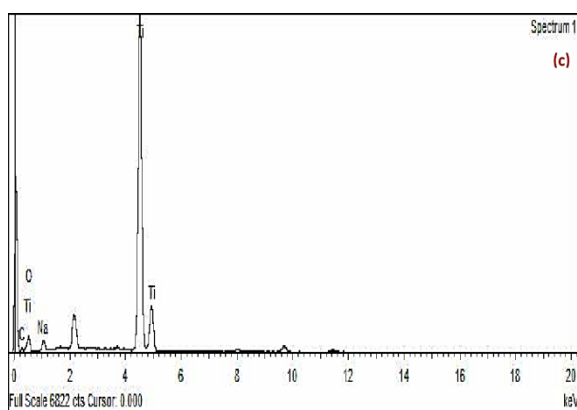
Fig. 3(b) FT-IR spectra of titanium dioxide calcined at 550 ºC (T-550 sample)

Fig. 4(a) FE-SEM micrograph of titanium dioxide calcined at 350 ºC (T-350 sample)

Fig. 4(b) FE-SEM micrograph of titanium dioxide calcined at 550 ºC (T-550 sample)

Fig. 4(c) EDX result of titanium dioxide sample.

4.2 The influence of initial dye concentration

One of the most critical parameters that affect the photodegradation process is the beginning dye concentration. The impact of various initial concentrations of MB dye (10, 15, and 20 mg/L) was studied on T-350 and T-550 photocatalysts, which were added to 50 mL of MB dye solutions. Fig. 8(ii), indicates that the lower concentrations of MB solutions have higher degradation rates. In Fig 8(ii) after 270 min of irradiation time, the degradation efficiency of 10 ppm over T-350 and T-550 reached 84.75 and 76.77%, respectively; 15 ppm MB over T-350 and T-550 reached 81.92 and 71.12%, respectively; and 20 ppm MB over T-350 and T-550 reached 80.16 and 69.68%, respectively. The cause of this could be that as MB concentration increases, the molecules can absorb light and decrease light transmission to the catalyst surface, making it difficult for the catalysts to absorb light energy. Additionally, excessive MB molecules will adhere to the catalyst surface, inhibiting the reaction of other substrates like H_2O_2, OH^-, and H_2O with the catalyst and the production of highly reactive radicals [35].

4.3 The influence of the photocatalyst dose

The photodegradation efficiency of MB over T-350 and T-550 photocatalysts is affected by variations of catalyst loadings. Accordingly, three different loadings (0.005, 0.01 and 0.02 g) of T-350 and T-550 photocatalysts were added to 50 mL of MB dye solutions and examined. The results are shown in Fig. 9(i-ii). Where the degradation performance is directly proportional to loading percent, reaching up to (89.60 and 84.53 %, respectively) for (T-350 and T-550) dye removal at 0.02 g within 270 min, reaching up to (88.05 and 81.62 %, respectively) for (T-350 and T-550) dye removal at 0.01 g within 270 min and reaching up to (84.75 and 76.17 %, respectively) for (T-350 and T-550) dye removal at 0.005 g within 270 min. The efficiency of photogeneration of electrons and holes was higher, which contributed to the increase in the contact area between solid and liquid. All these factors were advantageous in accelerating the reaction. This could be explained by the fact that as the dosage of photocatalyst was increased, more and more active sites were found on the photocatalyst surface [36].

4.4 The influence of the temperature

The temperature factor plays an important role and can affect the rate of photodegradation process. The photodegradation studies were performed at three different temperatures (294, 297 and 300 K) separately for MB dye removal using 0.005 g of T-350 and T-550 photocatalysts and a dye concentration of 15 mg/L in all samples. The experimental results showed that the removal percentage increased slowly with an increase in the solution temperature for MB dye, as shown in Fig. 10(i-ii). Over the examined temperature range, we concluded that with the increasing temperature of the dye solution, the removal percentage of the MB dye over the fabricated samples increased. The maximum removal efficiencies were obtained at a temperature of 300 K, which were 81.92 and 71.12%, respectively, for T-350 and T-550. One explanation for this is as follows: A higher temperature increases the thermal energy of molecules. Although there is an increased probability of collisions at higher temperatures, this alone accounts for a very small portion of the increase in reaction rate, and there are significantly more reactant molecules with enough energy to do so [37]. Additionally, this shows that the MB dye's photodegradation on the ready photocatalysts is an endothermic process. The findings indicate that a decreasing boundary layer thickness and an increase in temperature are occurring around the sorbent. As a result, the adsorbate's mass transfer resistance in the boundary layer decreased. This might have been brought on by the dye's increased mobility because of the temperature's higher kinetic energy. As a result, the dye photodegradation changed linearly with rising temperature.

4.5 Studies of photocatalyst recycling.

Under optimal conditions, recycling tests occurred to inquire into the recycling and photocatalytic stability of TiO_2 nanoparticles. Following the initial stage of the decomposition reaction cycle, the TiO_2 nanoparticles were extracted from the aqueous solution through the process of centrifugation, after which the treated wastewater was subsequently discharged. Subsequently, the photocatalyst that was separated was used again without undergoing any form of processing. The utilization of the photocatalytic process for the degradation of organic pollutants offers several benefits, including the ability to undergo several working cycles, thereby ensuring cost-effectiveness and sustained photocatalytic activity. Additionally, this process facilitates easy separation from the aqueous solution and enables the possibility of reuse. To evaluate the reuse of the photocatalysts, 1 g/L of TiO_2 calcined at different temperatures was added to 10 mg/L MB in 50 ml of aqueous solution and exposed to UV light for five consecutive cycles. After 5 cycles, the removal percent decreased with increasing cycle times for TiO_2, as shown in Fig. 11. The results have demonstrated that TiO_2 calcines at different temperatures. Photocatalysts offer great potential for photocatalytic activity with a highly efficient degradation rate and are stable and reusable after several treatment cycles, with a lower number of possible recycling cycles.
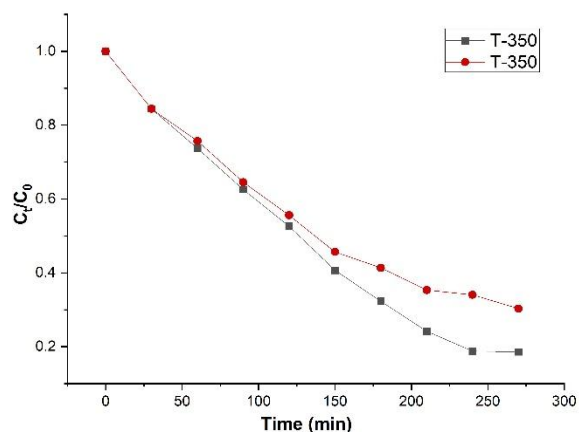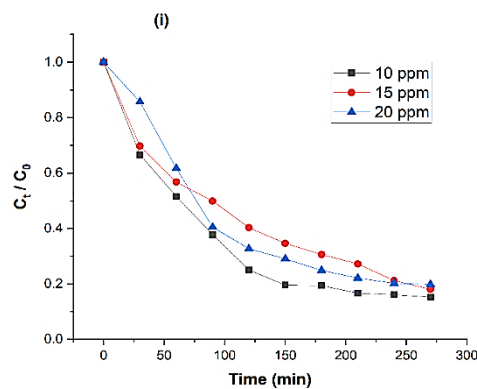
Fig. (5) illustrates the variation of C_t/C_0 of MB as a time function in the absence of graphene: T-350 and T-550 samples.
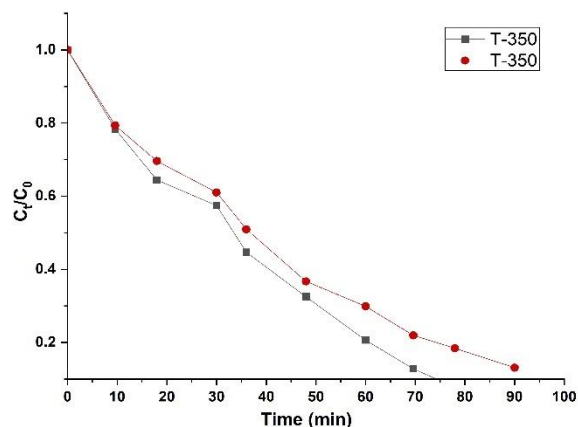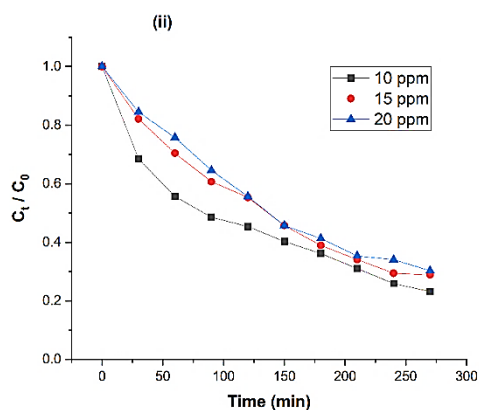
Fig. (6) illustrates the variation of C_t/C_0 of MB as a time function in the present of graphene: T-350 and T-550 samples.
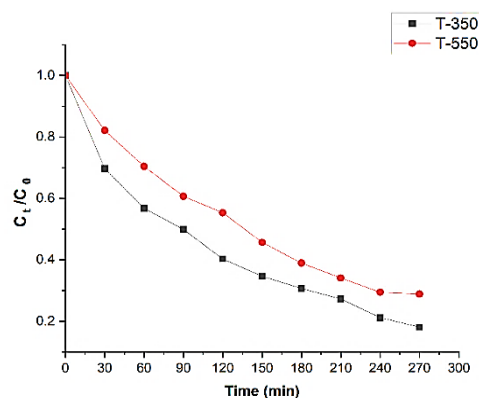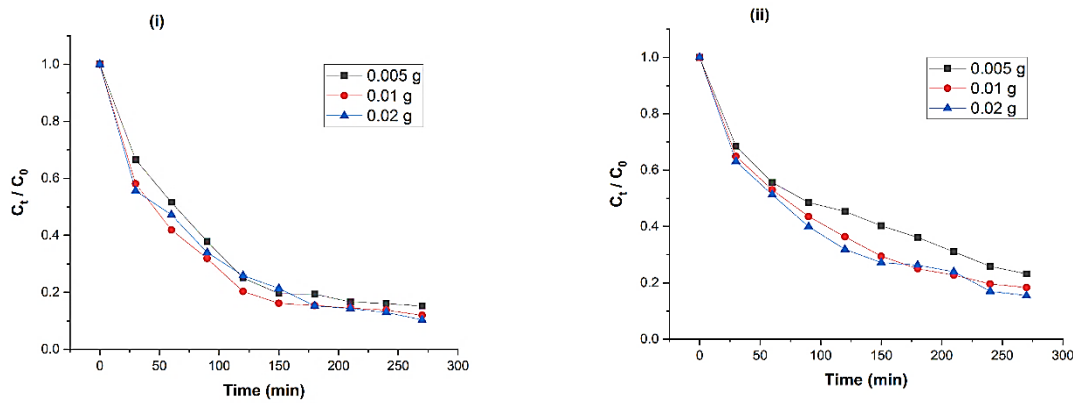
Fig. (7) Influence of contact time on the elimination of MB dye over T-350 and T-550 samples under UV light.
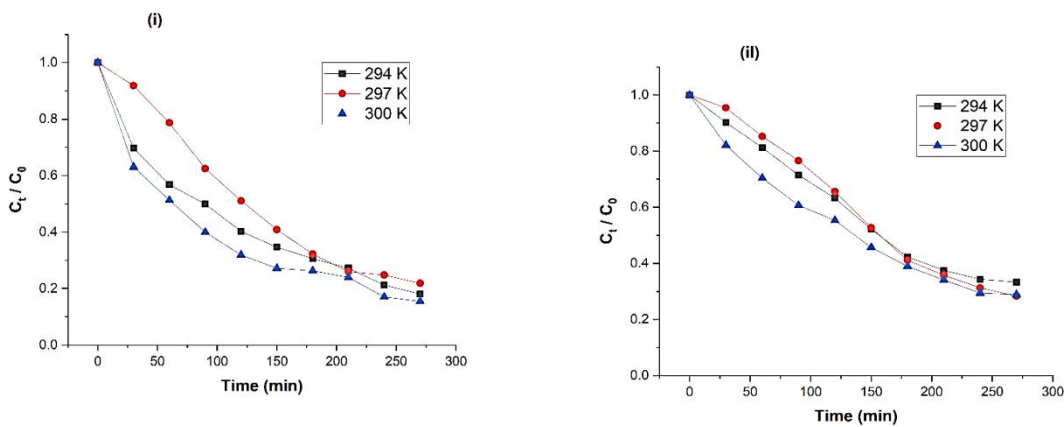
Fig. 8(i) Influence of the initial dye concentration on the elimination of MB dye over T-350 sample
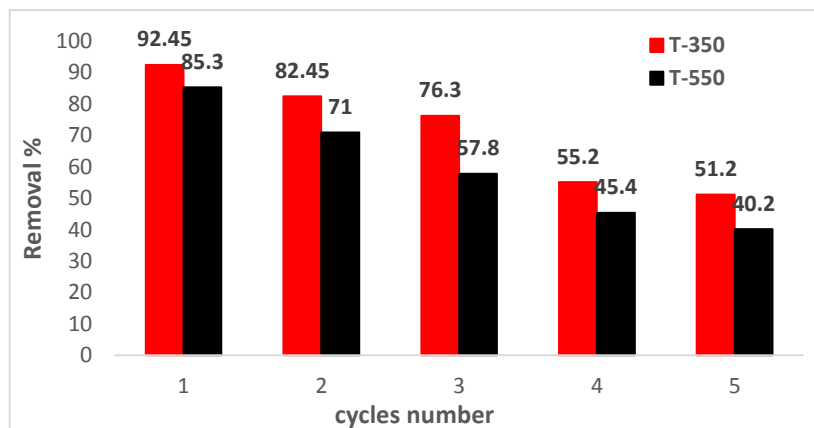
Fig. 8(ii) Influence of the initial dye concentration on the elimination of MB dye over T-550 sample

Fig. (9) Influence of photocatalyst dose on the elimination of MB dye over: **(i)**T-350 and **(ii)**T-550 samples.

Fig. (10) Influence of temperature on the elimination of MB dye using: **(i)**T-350 and **(ii)**T-550 samples.

Fig. (11) The recycling for the photodecomposition of MB dye using TiO_2 nanoparticles calcined at different temperatures (T-350 and T-550 samples).

5. kinetic studies

The photodegradation kinetic models were examined by studying the effect of contact time on the separation of MB dye over TiO_2 photocatalyst. Kinetic factors of the removal MB dye on TiO_2 nano photocatalyst were estimated using pseudo-first - order equation (plot ln (C_t/C_0) against t) [38] and pseudo-second-order equation (plot $(1/C_t)$- $(1/C_0)$ versus time t) [39] as represented in equations No. 2 and 3. Fig. 12 (i-ii) shows the kinetic studies for degradation MB over T-350 and T-550 photocatalysts.

$$ln(C_0 - C_t) = lnC_0 - \frac{K_1}{2.303} \qquad (2)$$

$$\frac{t}{C_t} = \frac{1}{K_2 C_0^2} + \frac{t}{C_0} \qquad (3)$$

where C_0 is the initial concentration of MB (mg L^{-1}), and C_t is the concentration of MB at time, t (mg L^{-1}), respectively, t (min) is contact time, and k_1 is a pseudo-first-order rate constant (min^{-1}) and k_2 (min^{-1} mmol^{-1}) is a pseudo- second-order rate constant. From Table. 1 and depending on the R^2 values, the pseudo-first-order model is better fitting than the pseudo-second order for the removal of the MB dye over TiO$_2$ nanoparticles calcined at different temperatures. So, we can say that the removal of MB dye over TiO$_2$ follows the pseudo-first-order model.
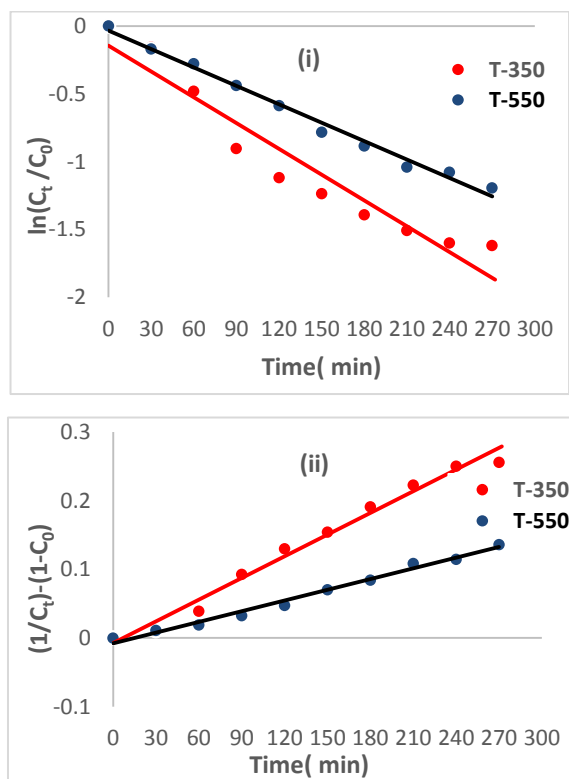
Fig. (12) Pseudo-first-order **(i)** and pseudo-second-order **(ii)** models for the removal of MB dye on TiO$_2$ nanoparticles calcined at different temperatures (T-350 and T-550 samples).

Table (1) Kinetic parameters for the photodecomposition of MB dye on TiO$_2$ photocatalyst

6. Thermodynamic studies

The reaction rate constant and removal efficiency of MB dye increase with increasing the reaction temperature for T-350 and T-550 for the photocatalytic degradation. The activation energy, which is a minimum energy needed for the reaction to occur, can be expressed by the Arrhenius equation [40]:

$$k_{app} = A e^{\frac{-E_a}{RT}} \qquad (4)$$

where k_{app} is the apparent rate constant for the first-order reaction (min^{-1}), A is the frequency factor (min^{-1}), E_a is the activation energy (kJ mol^{-1}) R is the ideal gas constant which is equal to 8.314 J K^{-1} mol^{-1} and T is the temperature (K). The equation's logarithm in linear form No. 4 can be written as:

$$\ln k_{app} = \ln A - \frac{E_a}{RT} \qquad (5)$$

The equation demonstrates the effect of a change in temperature on the rate constant. The calculated E_a obtained for the photodegradation of MB dye by T-350 and T-550 is presented in Table. 2(i-ii). According to transition state theory (TST), the Henry Eyring equation No. 6 can be used to conclude the temperature confidence on the apparent rate constant [37]:

$$K_{app} = \frac{K_B T}{h} \exp\left(\frac{-\Delta G^\circ}{RT}\right) \qquad (6)$$

Where K_B is the Boltzmann's constant which is equal to 1.3805×10-23 J K^{-1}, h is Planck's constant which is equal to 6.6261×10-34 J s and ΔG^0 is the normal Gibbs free energy transfer of activation (kJ mol^{-1}). In the thermodynamic property of TST, the standard enthalpy changes of activation (ΔH^0) and the standard entropy change of activation (ΔS^0) are brought together with the change in the normal Gibbs free energy transfer of activation equation as follows in Eq (7):

$$\Delta G^0 = \Delta H^0 - T \Delta S^0 \qquad (7)$$

By substituting of Eq (7) Eq (6), the linear form of Eyring's equation can be expressed as follows (8):

$$\ln\left(\frac{k_{app}}{T}\right) = \frac{-\Delta H^0}{RT} + \left(\ln\frac{k_B}{h} + \frac{\Delta S^0}{R}\right) \qquad (8)$$

The following expressions give an additional method of estimating it is possible to calculate the activation energy [41]:

$$E_a = \Delta H^0 + RT \qquad (9)$$

Therefore, a plot of dimensionless values of ln K_{app}h /K_BT) against 1/T provides a straight line and ΔH^0 and ΔS° are obtained from the slope and the intercept, respectively. The following expressions give an additional method of estimating the frequency factor and activation energy that can be computed [37]:

$$A = \frac{K_B T}{h} \exp\left(\frac{\Delta S^\circ}{R}\right) \qquad (10)$$

Fig. 14(i-ii) shows the Eyring plot of degradation of

Sample code	Pseudo 1st order kinetic parameters		Pseudo 2st order kinetic parameters	
	K_1 (min)$^{-1}$	R^2	K_2 (min^{-1} mmol^{-1})	R^2
T-350	0.005863	0.9849	0.0014906	0.9588
T-550	0.004751	0.9905	0.000917	0.9803

MB over T-350 and T-550 at different temperatures

and Table. 2(i-ii) provides the results of the computations of Arrhenius and TST theories for photocatalytic degradation of MB over T-350 and T-550. According to Table. 2(i-ii), the values of both $\Delta H°$ and $\Delta S°$ were found to be positive, while that of $\Delta G°$ was negative. The increasing value of k_{app} and the positive values of ΔH^0 with increasing temperature prove that the photocatalytic degradation of MB using T-350 and T-550 was an endothermic process The endothermic nature of the photocatalytic process is possibly due to the electrostatic interaction between the hydrophobic character of TiO_2 on the photocatalyst surface and organic pollutants. The hydrophobic surface property of TiO_2 photocatalyst favors the adsorption of organic pollutants onto charged TiO_2 surfaces to achieve efficient photocatalytic degradation and decreases agglomerations of nanoparticles [37]. The positive $\Delta S°$ value showed a high tendency to adsorb MB to

the catalyst and therefore a high degradation efficiency. The change of entropy ($\Delta S°$) reflects essentially the variation in the disorder of a system (on a macroscopic level) along a process. A higher level of variations at the connection between the solid and the solution, which may potentially involve some modifications to the structure of the sorbent and sorbate, is indicated by a positive value for this parameter. Moreover, $\Delta S° > 0$ indicates the degree of freedom of the species absorbed increased [42]. Finally, a negative side of $\Delta G°$ demonstrated the feasibility and automatic nature of the process, in which the system would go in the direction of producing reactants (a spontaneous process) [43]. Additionally, as the temperature increased, the G° values reduced, indicating that higher temperatures are slightly more favorable for the photocatalytic decomposition of MB dye.

Table 2(i) Thermodynamic parameters for the photodegradation of the MB dye using T-350 photocatalyst at different temperatures.

T, K	K_{app} (min^{-1})	Arrhenius theory		Transition state theory (TST)				
		E_a (KJ/mole)	R^2	ΔH^0 (KJ/mole)	ΔS^0 (KJ/K mole)	ΔG^0 (KJ/mole)	E_a (KJ/mole)	R^2
294	0.006120743	29.626	0.9994	27.12	0.10	-3.32	29.63	0.98
297	0.007024683					-3.744	29.66	
300	0.007964949					-4.01	29.69	

Table 2(ii) Thermodynamic parameters for the photodegradation of the MB dye using T-550 photocatalyst at different temperatures.

T, K	K_{app} (min^{-1})	Arrhenius theory		Transition state theory (TST)				
		E_a (KJ/mole)	R^2	ΔH^0 (KJ/mole)	ΔS^0 (KJ/K mole)	ΔG^0 (KJ/mole)	E_a (KJ/mole)	R^2
294	0.00311	32.65	0.9942	30.13	0.11	-1.36	32.57	0.999
297	0.004230533					-1.70	32.61	
300	0.005168624					-2.44	32.65	
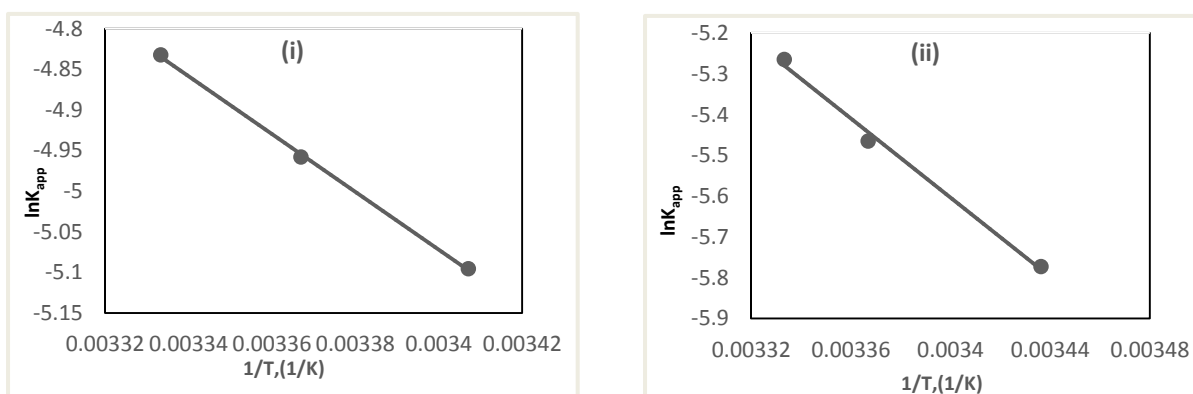
Fig.(13) The Arrhenius plot for calculating activation energy for the photodegradation of the MB dye using: **(i)**T-350 and **(ii)**T-550 samples.
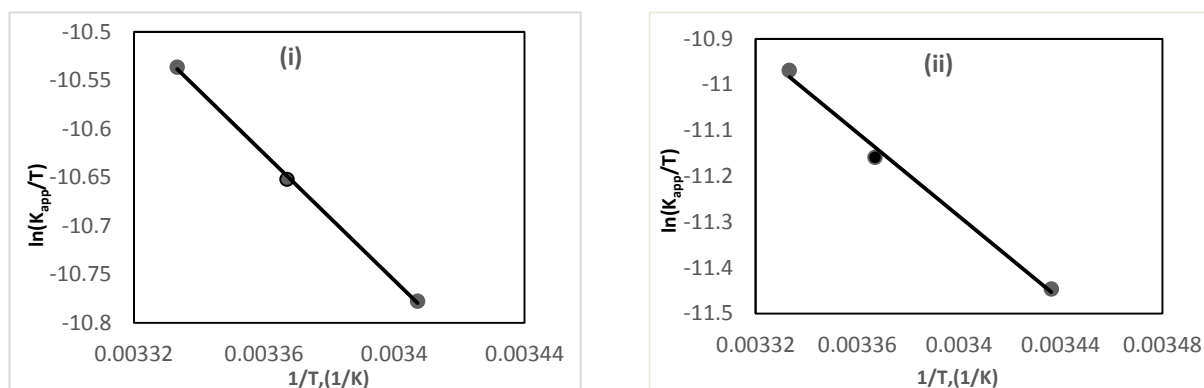
Fig. (14) Eyring plot for calculating thermodynamic parameters for the photodegradation of the MB dye using: (**i**)T-350 and (**ii**)T-550 samples.

7. Conclusion

In summary, we successfully prepared TiO_2 sea urchin-like structures with pointed spindles through a simple, one-step hydrothermal route. The synthesized product was characterized using various analytical approaches. The generated samples' photocatalytic reactions were evaluated using the hazardous MB dye under UV irradiation for 270 min. The T-350 sample shows better catalytic performance compared to the T-550 sample, which degrades up to 81.42% of MB dye under UV irradiation. As proposed from the route photocatalytic mechanism, we employed graphene (0.05 g) in the reaction system, to achieve further photocatalytic performance by enhancing the efficient separation and decreasing the electron-hole pair recombination rate. The degradation rate of MB dye over TiO_2 calcined at different temperatures (T-350 and T-550) was greatly enhanced by adding graphene, not only was the time of degradation decreased from 270 min to 90 min, but also the photocatalytic activity greatly increased to 95.84 and 86.9%, respectively. Furthermore, the prepared catalysts could be easily recovered and recycled up to five times with high catalytic activity. The photocatalytic properties of the synthesized product were investigated by studying different photocatalytic conditions such as contact time, initial dye concentrations, photocatalyst dosage and temperature. The photodegradation data showed that the photodegradation fits the pseudo-first-order model. Thermodynamic parameters for the photodegradation system showed that the photodegradation process is spontaneous, endothermic and favorable at high temperatures.

References

[1] T. Islam, M.R. Repon, T. Islam, Z. Sarwar, M.M. Rahman, Impact of textile dyes on health and ecosystem: A review of structure, causes, and potential solutions, Environmental Science and Pollution Research, 30 (2023) 9207-9242.

[2] B. Tan, Z. He, Y. Fang, L. Zhu, Removal of organic pollutants in shale gas fracturing flowback and produced water: A review, Science of The Total Environment, (2023) 163478.

[3] M.S.S. Abujazar, S.U. Karaağaç, S.S.A. Amr, M.Y. Alazaiza, M.J. Bashir, Recent advancement in the application of hybrid coagulants in coagulation-flocculation of wastewater: A review, Journal of Cleaner Production, 345 (2022) 131133. review, Advances in colloid and interface science, 272 (2019) 102009.

[7] C.H. Nguyen, C.-C. Fu, R.-S. Juang, Degradation of methylene blue and methyl orange by palladium-doped TiO_2 photocatalysis for water reuse: Efficiency and degradation pathways, Journal of Cleaner Production, 202 (2018) 413-427.

[8] K. Mahapatra, D. Ramteke, L. Paliwal, Production of activated carbon from sludge of food processing industry under controlled pyrolysis and its application for methylene blue removal, Journal of Analytical and Applied Pyrolysis, 95 (2012) 79-86.

[9] V. Augugliaro, M. Litter, L. Palmisano, J. Soria, The combination of heterogeneous photocatalysis with chemical and physical

[4] E. Hu, S. Shang, X.-m. Tao, S. Jiang, K.-l. Chiu, Regeneration and reuse of highly polluting textile dyeing effluents through catalytic ozonation with carbon aerogel catalysts, Journal of Cleaner Production, 137 (2016) 1055-1065.

[5] J. Dasgupta, J. Sikder, S. Chakraborty, S. Curcio, E. Drioli, Remediation of textile effluents by membrane-based treatment techniques: a state of the art review, Journal of environmental management, 147 (2015) 55-72.

[6] R. Gusain, K. Gupta, P. Joshi, O.P. Khatri, Adsorptive removal and photocatalytic degradation of organic pollutants using metal oxides and their composites: A comprehensive

operations: A tool for improving the photoprocess performance, Journal of Photochemistry and Photobiology C: Photochemistry Reviews, 7 (2006) 127-144.

[10] J.-M. Herrmann, Photocatalysis fundamentals revisited to avoid several misconceptions, Applied catalysis B: environmental, 99 (2010) 461-468.

[11] L. Zhu, G. Liu, X. Duan, Z.J. Zhang, A facile wet chemical route to prepare ZnO/TiO₂ nanotube composites and their photocatalytic activities, Journal of Materials Research, 25 (2010) 1278-1287.

[12] C.B. Ong, L.Y. Ng, A.W. Mohammad, A review of ZnO nanoparticles as solar photocatalysts: Synthesis, mechanisms and applications, Renewable and Sustainable Energy Reviews, 81 (2018) 536-551.

[13] Y. Jiang, Y. Luo, F. Zhang, L. Guo, L. Ni, Equilibrium and kinetic studies of CI Basic Blue 41 adsorption onto N, F-codoped flower-like TiO₂ microspheres, Applied Surface Science, 273 (2013) 448-456.

[14] K. Fan, T. Peng, J. Chen, X. Zhang, R. Li, A simple preparation method for quasi-solid-state flexible dye-sensitized solar cells by using sea urchin-like anatase TiO₂ microspheres, Journal of Power Sources, 222 (2013) 38-44.

[15] G. Zhou, Y. Zhao, C. Zu, A. Manthiram, Free-standing TiO₂ nanowire-embedded graphene hybrid membrane for advanced Li/dissolved polysulfide batteries, Nano Energy, 12 (2015) 240-249.

[16] G. Wang, Q. Wang, W. Lu, J. Li, Photoelectrochemical study on charge transfer properties of TiO₂− B nanowires with an application as humidity sensors, The Journal of Physical Chemistry B, 110 (2006) 22029-22034.

[17] L. Liu, P. Miao, Y. Xu, Z. Tian, Z. Zou, G. Li, Study of Pt/TiO₂ nanocomposite for cancer-cell treatment, Journal of Photochemistry and Photobiology B: Biology, 98 (2010) 207-210.

[18] T. Tachikawa, T. Majima, Metal oxide mesocrystals with tailored structures and properties for energy conversion and storage applications, NPG Asia Materials, 6 (2014) e100-e100.

[19] J. Yan, G. Wu, N. Guan, L. Li, Z. Li, X. Cao, Understanding the effect of surface/bulk defects on the photocatalytic activity of TiO₂: anatase versus rutile, Physical Chemistry Chemical Physics, 15 (2013) 10978-10988.

[20] P.K. Narayanam, S. Major, Langmuir-Blodgett based growth of rGO wrapped TiO₂ nanostructures and their photocatalytic performance, Colloids and Surfaces A: Physicochemical and Engineering Aspects, 609 (2021) 125652.

[21] N. Venkatachalam, M. Palanichamy, V. Murugesan, Sol–gel preparation and characterization of nanosize TiO₂: Its photocatalytic performance, Materials Chemistry and Physics, 104 (2007) 454-459.

[22] S. Zhan, Y. Yang, X. Gao, H. Yu, S. Yang, D. Zhu, Y. Li, Rapid degradation of toxic toluene using novel mesoporous SiO₂ doped TiO₂ nanofibers, Catalysis Today, 225 (2014) 10-17.

[23] K. Chen, Z. Jiang, J. Qin, Y. Jiang, R. Li, H. Tang, X. Yang, Synthesis and improved photocatalytic activity of ultrathin TiO₂ nanosheets with nearly 100% exposed (001) facets, Ceramics International, 40 (2014) 16817-16823.

[24] K. Hayashi, M. Nakamura, Y. Makita, R. Fujiwara, T. Kori, K. Ishimura, Synthesis and photocatalytic activity of sea urchin-shaped rutile TiO₂ nanocrystals, Materials Letters, 65 (2011) 3037-3040.

[25] L. Xiang, X. Zhao, C. Shang, J. Yin, Au or Ag nanoparticle-decorated 3D urchin-like TiO₂ nanostructures: Synthesis, characterization, and enhanced photocatalytic activity, Journal of colloid and interface science, 403 (2013) 22-28.

[26] Z. Wu, Q. Wu, L. Du, C. Jiang, L. Piao, Progress in the synthesis and applications of hierarchical flower-like TiO₂ nanostructures, Particuology, 15 (2014) 61-70.

[27] D. Fattakhova-Rohlfing, A. Zaleska, T. Bein, Three-dimensional titanium dioxide nanomaterials, Chemical reviews, 114 (2014) 9487-9558.

[28] F. Hashemzadeh, M. Mehdi Kashani Motlagh, A. Maghsoudipour, A comparative study of hydrothermal and sol–gel methods in the synthesis of MnO₂ nanostructures, Journal of sol-gel science and technology, 51 (2009) 169-174.

[29] K.P. Cabral, W. Kurniawan, H. Hinode, Three-dimensional sea urchin-like TiO₂ synthesized via facile hydrothermal method: Its properties and solar photocatalytic activity, Journal of Environmental Chemical Engineering, 3 (2015) 2786-2796.

[30] G. Polat, Y.S. Açıkel, Synthesis and characterization of magnetic halloysite–alginate beads for the removal of lead (II) ions from aqueous solutions, Journal of Polymers and the Environment, 27 (2019) 1971-1987.

[31] W. Zhou, Y. He, Ho/TiO₂ nanowires heterogeneous catalyst with enhanced photocatalytic properties by hydrothermal synthesis method, Chemical Engineering Journal, 179 (2012) 412-416.

[32] B. Santara, P. Giri, Impact of reaction temperature, stirring and cosolvent on the solvothermal synthesis of anatase TiO₂ and TiO₂/titanate hybrid nanostructures:

elucidating the growth mechanism, Materials Chemistry and Physics, 137 (2013) 928-936.

[33] A. Gemeay, M. El-Halwagy, Immobilization impact of photocatalysts onto graphene oxide, Graphene Oxide-Applications and Opportunities, IntechOpen London, UK2018, pp. 13563-13570.

[34] S. Stankovich, D.A. Dikin, R.D. Piner, K.A. Kohlhaas, A. Kleinhammes, Y. Jia, Y. Wu, S.T. Nguyen, R.S. Ruoff, Synthesis of graphene-based nanosheets via chemical reduction of exfoliated graphite oxide, carbon, 45 (2007) 1558-1565.

[35] N.A. Barakat, M.A. Kanjwal, I.S. Chronakis, H.Y. Kim, Influence of temperature on the photodegradation process using Ag-doped TiO_2 nanostructures: negative impact with the nanofibers, Journal of Molecular Catalysis A: Chemical, 366 (2013) 333-340.

[36] K. Byrappa, A. Subramani, S. Ananda, K.L. Rai, R. Dinesh, d.M. Yoshimura, Photocatalytic degradation of rhodamine B dye using hydrothermally synthesized ZnO, Bulletin of materials science, 29 (2006) 433-438.

[37] K. Byrappa, A. Subramani, S. Ananda, K.L. Rai, R. Dinesh, d.M. Yoshimura, Photocatalytic degradation of rhodamine B dye using hydrothermally synthesized ZnO, Bulletin of materials science, 29 (2006) 433-438.

[38] B.E. Reed, M.R. Matsumoto, Modeling cadmium adsorption by activated carbon using the Langmuir and Freundlich isotherm expressions, Separation science and technology, 28 (1993) 2179-2195.

[39] G.P. Jeppu, T.P. Clement, A modified Langmuir-Freundlich isotherm model for simulating pH-dependent adsorption effects, Journal of contaminant hydrology, 129 (2012) 46-53.

[40] K. Chen, Z. Jiang, J. Qin, Y. Jiang, R. Li, H. Tang, X. Yang, Synthesis and improved photocatalytic activity of ultrathin TiO_2 nanosheets with nearly 100% exposed (001) facets, Ceramics International, 40 (2014) 16817-16823.

[41] H.S. Wahab, A.A. Hussain, Photocatalytic oxidation of phenol red onto nanocrystalline TiO_2 particles, Journal of Nanostructure in Chemistry, 6 (2016) 261-274.

[42] C. Escudero-Oñate, I. Villaescusa, The thermodynamics of heavy metal sorption onto lignocellulosic biomass, Heavy metals, IntechOpen2018.

[43] F. Amiri, M. Dehghani, Z. Amiri, S. Yousefinejad, A. Azhdarpoor, Photocatalytic degradation of 2, 4-dichlorophenoxyacetic acid from aqueous solutions by Ag_3PO_4/TiO_2 nanoparticles under visible light: kinetic and thermodynamic studies, Water Science and Technology, 83 (2021) 3110-3122.